Solely extension-related origin of the eastern to west-central Mexican Volcanic Belt (Mexico) from partial melting inversion model

Surendra P. Verma

Centro de Investigación en Energía, UNAM, Priv. Xochicalco s/no., Col. Centro, Apartado Postal 34, Temixco, Morelos 62580 Mexico

Southern Mexico presents a unique volcano-tectonic situation on earth where the Mexican Volcanic Belt (MVB) – a Miocene to Recent volcanic province – is located. Its origin has been highly controversial because a diversity of opposing hypotheses, varying from a conventional subduction-relationship, through hybrid models, to the other extreme of extensional-relationship or rifting, has been proposed. I present results of the partial melting inversion model for geochemical data of basic rocks from the eastern to west-central MVB, which constrain its origin in terms of a pure extensional-relationship from a mantle source unaffected by the subduction of the Cocos plate beneath the North American plate. If the Cocos plate does contribute to the magma genesis in this area, the rocks from the 'front-arc', i.e. from closer to the trench, should show a clearer geochemical subduction signal than those from the 'back-arc' region, i.e. farther from the trench, which is clearly not observed, confirming a mantle origin for the MVB.

A rather unique and surprising geological situation has been recently discovered in southern Mexico[1] where, in spite of ongoing subduction of the Cocos plate into the Middle America Trench (MAT) beneath the Pacific coast of Mexico (Figure 1), the subducting slab does not seem to give rise to any volcanism on-land in the Mexican region. Instead, this south Mexican volcanism is interpreted to be related to the ongoing extension[1]. For Central American volcanoes, on the other hand, a clear subduction-relationship has been established between the same subducting Cocos plate and the Caribbean plate (Figure 1)[2,3].

There are two major Miocene to Recent volcanic provinces in this area: Mexican Volcanic Belt (MVB) in southern Mexico and Central American Volcanic Arc (CAVA) in Central America (Figure 1). Although the CAVA is subparallel to the trench, the MVB makes an angle of about 20° with it (Figure 1), so that the 'volcanic front' in the eastern part of the MVB, corresponding to the subduction of the Cocos plate, is about 480 km from the MAT and in the west-central part, it is only about 220 km from it. The seismicity, gravity, thermal, geological and geochemical data are all anomalous ('rift-like' instead of 'arc-like') beneath the MVB[1,4–14].

e-mail: spv@cie.unam.mx

Besides the uniqueness of south Mexican volcanism, this trench is also unique in its morphology: north of the Tehuantepec Ridge system (see Te-Ri in Figure 1), the continental shelf is narrow and much of the continental margin is a steep continental slope, whereas, south of this ridge, the continental shelf is underlain by a wide fore-arc basin[15].

At least in the western part of the MVB (Figure 1), there exists a well-developed rift system consisting of three major rifts: north-west-trending Tepic–Zacoalco Rift, north-south-trending Colima Rift, and east-west-trending Chapala Rift[16–18]. The latter extends into the west-central part of the MVB and probably beyond this area into its east-central and eastern parts, because graben or extensional structures have been mapped throughout the belt[13,19–21]. Besides this triple rift system, a small oceanic plate – the Rivera plate – has been subducting beneath the western MVB, which may also exert an influence on the origin of volcanism in this region[6,22,23] (Figure 1).

The origin of the MVB, being a major belt of volcanism in southern Mexico (Figure 1), has been controversial; the models vary from the conventional relationship of subduction of the Cocos and Rivera plates under the North American plate[13,24–28], to hybrid models involving both mantle and slab sources[6,23,29], to the trace of passage of the North American plate over a mantle plume[7], and more recently, to the ongoing extensional processes throughout the belt[1,9,21,30].

These diverse varieties of hypotheses contrast with the conventional subduction-relationship of the volcanism in

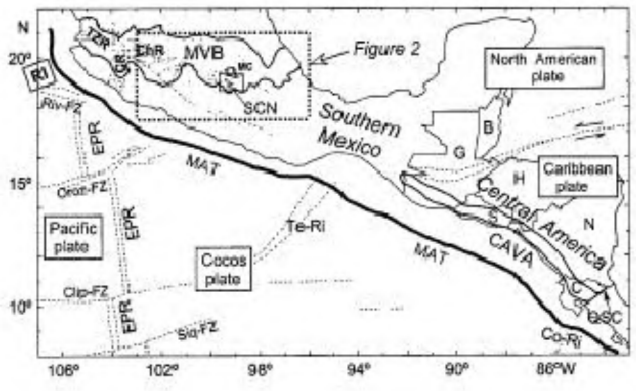

Figure 1. Location and present tectonic setting of the Mexican Volcanic Belt (MVB) and the Central American Volcanic Arc (CAVA), modified after Verma[1]. The plate tectonic relationship of the subducting Cocos plate with the North American and Caribbean plates is also shown. RI, Rivera plate (a small oceanic plate, north of the Cocos plate); MAT, Middle America Trench; EPR, East Pacific Rise; Riv-FZ, Rivera Fracture Zone; Oroz-FZ, Orozco Fracture Zone; Clip-FZ, Clipperton Fracture Zone; Siq-FZ, Siqueiro Fracture Zone; Te-Ri, Tehuantepec Ridge; Co-Ri, Cocos Ridge; QSC, Quesada Sharp Contortion; TZR, NW-SE-oriented Tepic-Zacoalco Rift system; CR, N-S-oriented Colima Rift system; ChR, E-W-oriented Chapala Rift system; SCN, Sierra de Chichinautzin monogenetic volcanic field; MC, Mexico City. The box marked 'Figure 2' is the area shown in Figure 2. The countries in Central America shown on this map are: G, Guatemala; B, Belize; S, El Salvador; H, Honduras; N, Nicaragua; C, Costa Rica.

Central America from Guatemala to north-western Costa Rica[2,3] (CAVA – north of QSC – in Figure 1). The controversies related to the origin of the MVB have now grown to such an extent that some authors are even modifying the long accepted name of this volcanic belt (Mexican Volcanic Belt), calling it 'Mexican Volcanic Arc'[28], or denominating the extension within the belt as 'intra-arc extension'[13], or referring to the area of some local studies as 'behind-the-arc', with no indication of where the corresponding arc is located[31,32], whereas others[1,9–12,14,21,30,33–35] are relating its origin to purely extensional or rift-related processes, probably implying a new name 'Mexican Volcanic Rift' for this belt.

New constraints are, therefore, still required to resolve this controversy. I present here the first partial melting inversion model for the eastern to west-central MVB, based on an exhaustive collection of geochemical data on basic rocks ($SiO_2 < 52\%$) from this area. Although on a relatively local basis, an inversion model has recently been

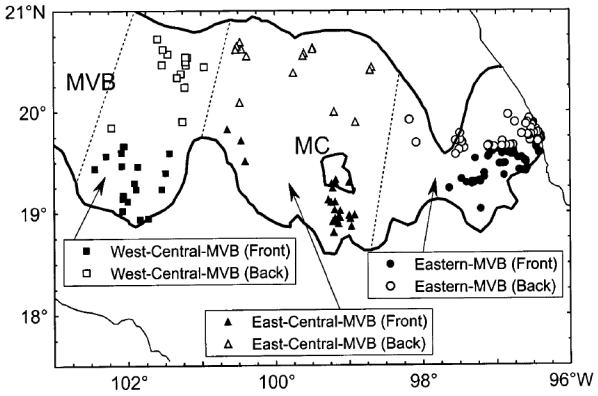

Figure 2. Simplified map showing sample locations. Symbols based on an 'assumed arc system' highlight the distribution of basic rocks in the MVB. Filled symbols are used for 'volcanic front' or 'front-arc' rocks, whereas open symbols are used for the 'behind the volcanic front' or 'back-arc' region. MC (Mexico city) shows the largest (highest population) city of the world. Approximate division of the area of study in shown by dotted lines as eastern MVB, east-central MVB, and west-central MVB.

Table 1. Linear regression coefficients for trace-element inverse-modelling results for all basic rock samples ($SiO_2 < 52\%$) from the west-central to eastern Mexican Volcanic Belt, using Rb as a reference element (the most highly incompatible element)

Element		$(C^{Rb}–C^i)_E$ diagram						$(C^{Rb}–C^{Rb}/C^i)_E$ diagram					
(i)	n	m^i	se_{mi}	I^i	se_{Ii}	r	$P_{c(r,n)}$	m^i	se_{mi}	I^i	se_{Ii}	r	$P_{c(r,n)}$
La	77	0.62	0.07	15.6	2.9	0.704	< 0.0001	0.0096	0.0022	0.64	0.09	0.454	< 0.0001
Ce	76	0.47	0.06	14.8	2.4	0.678	< 0.0001	0.0132	0.0024	0.68	0.09	0.546	< 0.0001
Pr	53	0.38	0.05	11.5	2.1	0.717	< 0.0001	0.0161	0.0035	0.87	0.14	0.545	< 0.0001
Nd	69	0.305	0.040	11.0	1.6	0.679	< 0.0001	0.0210	0.0033	0.89	0.13	0.618	< 0.0001
Sm	69	0.187	0.025	8.4	1.0	0.671	< 0.0001	0.033	0.005	1.16	0.18	0.666	< 0.0001
Eu	70	0.121	0.020	8.2	0.8	0.595	< 0.0001	0.049	0.005	1.10	0.22	0.736	< 0.0001
Gd	53	0.098	0.023	7.3	0.9	0.515	< 0.0001	0.059	0.008	1.25	0.31	0.731	< 0.0001
Tb	70	0.065	0.016	6.7	0.6	0.441	0.0001	0.080	0.008	1.18	0.31	0.778	< 0.0001
Dy	40	0.029	0.009	6.54	0.43	0.453	0.0034	0.06	0.10	0.94	0.33	0.922	< 0.0001
Ho	53	0.032	0.016	5.6	0.6	0.275	*0.0460**	0.130	0.013	0.9	0.5	0.824	< 0.0001
Er	53	0.023	0.015	5.4	0.6	0.216	*0.1205**	0.154	0.013	0.6	0.5	0.863	< 0.0001
Tm	38	0.076	0.024	3.4	0.8	0.465	0.0033	0.149	0.028	1.2	0.8	0.668	< 0.0001
Yb	69	0.019	0.011	4.80	0.43	0.215	*0.0766**	0.181	0.012	0.39	0.48	0.879	< 0.0001
Lu	69	0.017	0.010	4.75	0.39	0.207	*0.0873**	0.185	0.012	0.39	0.46	0.890	< 0.0001
B	14	0.06	0.08	16	4	0.205	*0.4831**	0.032	0.006	0.97	0.28	0.846	0.0001
Ba	164	0.82	0.12	37	5	0.485	< 0.0001	0.0062	0.0007	0.366	0.033	0.561	< 0.0001
Be	24	0.24	0.08	17.0	3.7	0.564	0.0041	0.019	0.006	0.82	0.27	0.590	0.0024
Cs	45	1.02	0.10	– 5.7	4.3	0.848	< 0.0001	– 0.001	0.005	1.41	0.20	0.025	*0.8715**
Ga	57	0.017	0.005	4.45	0.22	0.408	< 0.0001	0.173	0.009	0.85	0.38	0.937	< 0.0001
Hf	49	0.129	0.023	11.7	1.0	0.624	< 0.0001	0.0384	0.0037	0.78	0.16	0.836	< 0.0001
Nb	155	0.34	0.06	15.3	2.7	0.428	< 0.0001	0.020	0.005	0.93	0.22	0.331	< 0.0001
Pb	115	0.17	0.07	32.0	3.3	0.235	0.0114	0.0213	0.0029	0.37	0.14	0.566	< 0.0001
Sr	167	0.149	0.041	26.1	1.9	0.271	0.0004	0.0492	0.0014	0.39	0.07	0.775	< 0.0001
Ta	43	0.28	0.09	20.0	4.0	0.430	0.0040	0.021	0.005	0.58	0.24	0.516	0.0004
Th	92	0.66	0.10	17	5	0.563	< 0.0001	0.0059	0.0028	0.92	0.15	0.215	0.0400
U	48	1.03	0.09	7.3	3.8	0.871	< 0.0001	0.0022	0.0014	0.76	0.06	0.222	*0.1295**
Y	162	0.027	0.006	5.66	0.28	0.331	< 0.0001	0.127	0.005	0.89	0.21	0.911	< 0.0001
Zr	166	0.118	0.021	13.6	0.9	0.403	< 0.0001	0.042	0.003	0.61	0.14	0.739	< 0.0001
Ti	168	0.030	0.009	7.89	0.41	0.250	0.0011	0.100	0.005	0.62	0.22	0.842	< 0.0001
P	168	0.274	0.038	13.2	1.7	0.493	< 0.0001	0.0215	0.0022	0.89	0.10	0.609	< 0.0001
K	170	0.42	0.05	26.6	2.1	0.576	< 0.0001	0.0193	0.0015	0.17	0.07	0.701	< 0.0001

n, Number of data pairs considered in the trace-element diagrams; m^i, Slope of the linear model; I^i, Intercept value of the linear model; r, Correlation coefficient of the linear model; $P_{c(r,n)}$, Probability that the variables are not correlated (i.e. $[1\text{-}P_{c(r,n)}]$ is the probability that the two variables are correlated); se_{mi}, Standard error for slope in $(C^{Rb}–C^i)_E$ or $(C^{Rb}–C^{Rb}/C^i)_E$ diagram; se_{Ii}, Standard error for intercept in $(C^{Rb}–C^i)_E$ or $(C^{Rb}–C^{Rb}/C^i)_E$ diagram; subscript E refers to normalization with respect to silicate earth values. All concentration data are normalized against silicate earth values (in ppm) by McDonough and Sun[47]: La = 0.648; Ce = 1.675; Pr = 0.254; Nd = 1.250; Sm = 0.406; Eu = 0.154; Gd = 0.544; Tb = 0.099; Dy = 0.674; Ho = 0.149; Er = 0.438; Tm = 0.068; Yb = 0.441; Lu = 0.0675; B = 0.30; Ba = 6.600; Be = 0.068; Cs = 0.021; Ga = 4.0; Hf = 0.283; Nb = 0.658; Rb = 0.600; Sr = 19.9; Ta = 0.037; Th = 0.0795; U = 0.0203; Y = 4.30; Zr = 10.5; Ti = 1205; P = 90; K = 240. *denotes statistically invalid correlations even at the 95% confidence level (italicized $P_{c(r,n)}$ values).

presented for the Sierra de Chichinautzin (SCN) area supporting a rift-related origin[14], this is an inversion study for the entire region of the eastern to west-central MVB.

The database includes geochemical and radiogenic isotope data on 196 samples of basic rocks, presented by several workers[1,11,12,14,25,27,29,31–41]. The present database is much more extensive than the one used recently by Verma[1]. Basic rocks are used for this purpose to minimize the effects of differentiation processes such as fractional crystallization and crustal contamination. Sample locations summarized in Figure 2 show the distribution of these rocks as 'volcanic front' (front-arc) or 'behind the volcanic front' (back-arc) rocks. This nomenclature and subdivision is used to test from inverse modelling, a conventional subduction-related origin of the MVB.

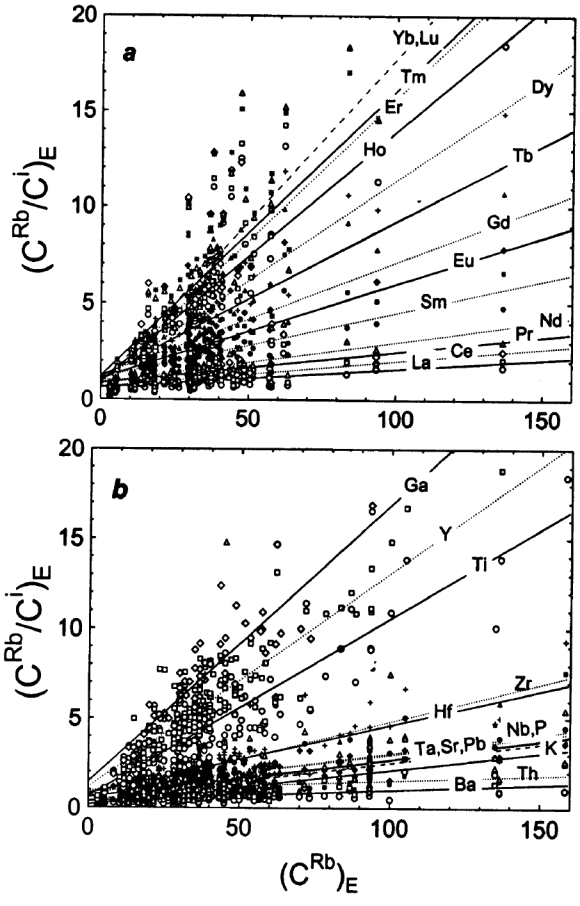

Figure 3. Diagrams of C^{Rb}/C^i against C^{Rb} (i being an incompatible trace element) for the MVB basic magmas. ***a***, REE plots; ***b***, LILE (Ba, K, and Sr) and HFSE (Th, Ta, Nb, Zr, Hf, Ti, and P), Y (a REE), and Ga plots. All concentration data were normalized against silicate earth values proposed by McDonough and Sun[47]. These values are: La = 0.648; Ce = 1.675; Pr = 0.254; Nd = 1.250; Sm = 0.406; Eu = 0.154; Gd = 0.544; Tb = 0.099; Dy = 0.674; Ho = 0.149; Er = 0.438; Tm = 0.068; Yb = 0.441; Lu = 0.0675; Rb = 0.600; Ba = 6.600; Sr = 19.9; Cs = 0.021; K = 240; Nb = 0.658; Ta = 0.037; Zr = 10.5; Hf = 0.283; Th = 0.0795; U = 0.0203; Ti = 1205; P = 90; Y = 4.30; and Ga = 4.0. Parameters of the least-squares linear regressions (slopes m^i, intercepts I^i, correlation coefficients r and probability estimates $P_{c(r,n)}$) are summarized in Table 1.

When a series of near-primary basic magmas are available, inverse modelling could be useful for inferring source characteristics from the variations in trace element concentrations of a suite of rocks produced by different degrees of melting[42–46]. The method of inverse modelling is the same as that proposed by Hofmann and Feigenson[42] and was used by Ormerod *et al.*[43] for the Big Pine volcanic field, California and by Velasco-Tapia and Verma[14] for the SCN area (Figure 1). The relevant equations have already been discussed, and the reader is referred to any of these papers.

The isotopic compositions of the MVB basic magmas, although not totally uniform, show relatively narrow ranges[1], and therefore, can be used for inverse modelling. For the basic rocks compiled in this database, some fractionation of olivine must have taken place from the mantle en route to the surface, but this is not likely to significantly change the trace element ratios of highly incompatible elements, on which inverse modelling is based. Further, the magmas should strictly be cogenetic and related to different degrees of melting of the same source,

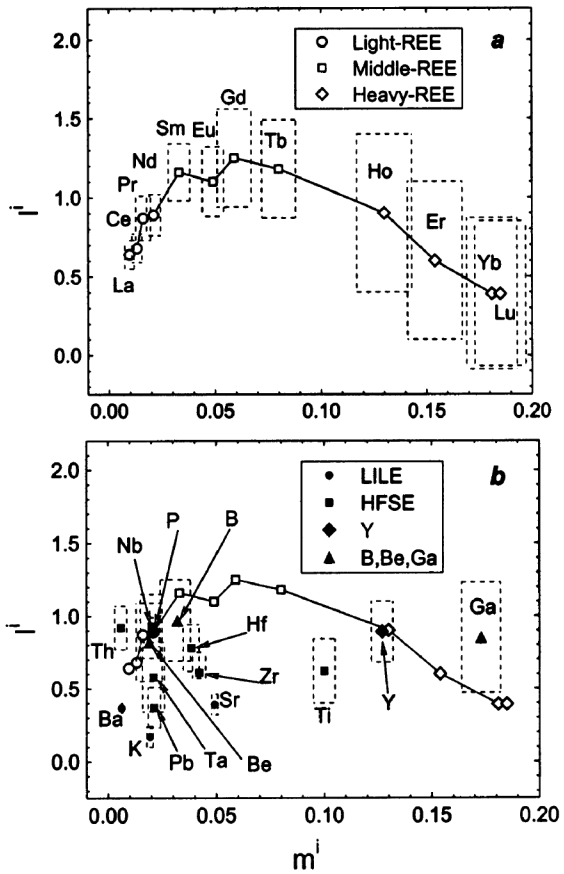

Figure 4. Diagrams of m^i–I^i for all basic magmas from the eastern to west-central MVB. ***a***, REE (La to Lu) and ***b***, LILE (Ba, K, and Sr), HFSE (Nb, Ta, Th, Zr, Hf, Ti, and P), Y (a REE), B, Be, and Ga. The size of each rectangle (dotted lines) represents one standard error on the regression parameters, derived from the C^{Rb}–C^{Rb}/C^i diagrams (Figure 3). For comparison, in addition to the rest of the trace-elements, REE data are also represented in ***b***.

which probably requires that the data be inverted independently for each local area. Unfortunately, this 'local inversion' is not possible at present because only generally incomplete datasets are available for a limited number of basic rock samples from a given locality, resulting in 'statistical samples' of inappropriately small size, unsuitable for an inverse modelling. In spite of these difficulties, it is useful to invert the data as a whole for inferring average source characteristics for this province and for examining if any contribution from the subducted Cocos plate can be seen in the eastern to west-central MVB.

Rb is used here as the most incompatible element, instead of La as employed by Velasco-Tapia and Verma[14], simply because Rb data by XRF (X-ray fluorescence) are considered more precise than La values by the same analytical method and, in the database, more Rb-trace element paired data are available than La-trace element pairs. The results of linear regression element–element $(C^{Rb}–C^{i})_E$ and element–element ratio $(C^{Rb}–C^{Rb}/C^{i})_E$ equations (where superscript i refers to a trace element other than Rb and subscript E refers to normalization with respect to silicate earth – concentration values used were those estimated by McDonough and Sun[47]) for all MVB data are presented in Table 1 and Figure 3. For rare-earth elements (REE) with statistically valid correlations $(C^{Rb}–C^{Rb}/C^{i})_E$ at the 99% confidence level, the incompatibility decreases in the sequence from La (light-REE) to Lu (heavy-REE); for other trace elements, the incompatibility sequence is Rb > Ba ~ Th > K > Ta ~ Sr ~ Pb ~ Nb ~ P > Hf ~ Zr > Ti > Y > Ga (Table 1, Figure 3). The slope m^i – intercept I^i plots (Figure 4) show that all high-field strength elements (HFSE), viz. Nb, Zr, Ta, Hf, Pb, Th, Ti, and P fall close to the REE trend represented by the solid line. The HFSE also fall close to the large ion lithophile elements (LILE: Ba, K, and Sr). The similarity of HFSE with REE and LILE in Figure 4 implies that the source of the MVB magmas is not depleted in any of the HFSE compared to the REE and LILE. For comparison, it is interesting to point out that Ormerod *et al.*[43] observed in the Big Pine volcanic field of California that the HFSE (Nb, Ta, Zr, and Hf) plotted well above their REE curve, in the region of low to moderate slope combined with a high intercept (i.e. in the upper left corner of m^i–I^i diagram, Figure 4 *b*). From partial melting equations it can be shown that for a source depleted in the HFSE compared to the REE and LILE, this would be the case, i.e. the HFSE would fall in the upper left part of the diagram (Figure 4), away from the LILE and REE. Ormerod *et al.*[43] interpreted their results as consistent with low source abundance of these HFSE compared to the REE and LILE in their study area.

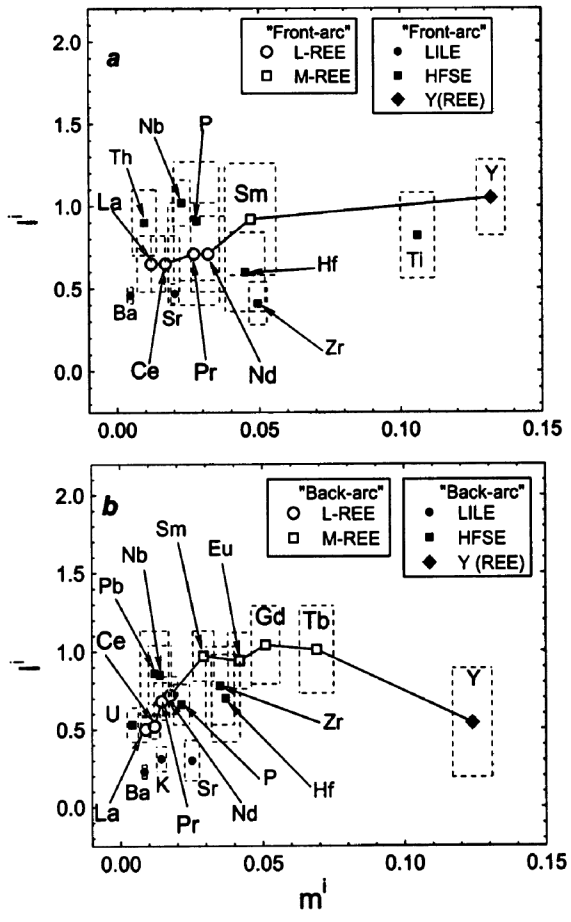

Figure 5. Diagrams of m^i–I^i for basic magmas from the eastern to west-central MVB. ***a***, REE, LILE, HFSE and Y for the 'volcanic front' or 'front-arc' magmas (locations shown by filled symbols in Figure 2). ***b***, REE (La to Lu) and LILE, HFSE and Y for the 'behind the volcanic front' or 'back-arc' magmas (locations shown by open symbols in Figure 2). For the size of each rectangle (dotted lines), see explanation in Figure 4.

If there is any contribution of the subducted slab in the genesis of MVB basic magmas, it should be observable more easily in rocks from the 'front-arc' compared to those from the 'back-arc' region, for which two tests were used: (i) to carry out inversion of data for rocks from the 'front-arc' and 'back-arc' areas separately in order to check if the former shows a clearer slab signature than the latter and (ii) to compute statistical parameters of rock chemistry from different areas of the MVB, distinguishing the 'front-arc' and 'back-arc' rocks from each region, and to compare the results among different segments as well as with the subduction-related CAVA.

The results for the MVB rocks (Figure 2) are synthesized in Figure 5 *a* for 'front-arc' magmas and Figure 5 *b* for 'back-arc' magmas (tabulated data are not shown here). It is clear that there is no significant fractionation of the HFSE from the REE and LILE, because the HFSE lie close to the REE curve and LILE data. If there were any significant contribution from the subducted Cocos plate, at least the 'front-arc' magmas would have shown a depletion of the HFSE in the source with respect to the REE and LILE, i.e. the HFSE should fall in the upper left corner of the diagram, which is clearly not observed in Figure 5 *a* and *b* (for an example of such a depletion, see Ormerod *et al.*[43]).

It is possible to go a step further and estimate, under certain assumptions, the actual composition of the mantle source region. However, it would not be worthwhile to do so until more complete datasets become available for most of these magmas (see widely different '*n* values' in Tables 1 and 2 for different elements or element pairs) and for a larger number of geological samples from any given locality (see the actual distribution of samples in Figure 2).

An alternative way is to examine the statistical information on selected geochemical parameters from our database separately for three segments (Figure 2) and for the entire MVB (Table 2) as well as to compare the results with those for the CAVA. $(SiO_2)_{Adj}$ values were included to simply show that the rocks compiled in the database are all basic rocks and this parameter does not vary significantly in the compiled rocks. There are no statistically significant differences in the MVB for key trace element ratios (La/Yb, Ba/La, Ba/Zr and Ba/Nb), particularly for two new parameters ($LILE_E/LREE_E$ showing LILE enrichment with respect to light-REE, and $LILE_E/HFSE_E$ show-

Table 2. Statistical information of selected chemical parameters for basic magmas from the eastern to west-central Mexican Volcanic Belt and comparison with the Central American Volcanic Arc

	Volcanic front or front-arc				Behind the volcanic front or back-arc			
Element	*n*	$x \pm s$	99%CL	Range	*n*	$x \pm s$	99%CL	Range
				Eastern segment				
$(SiO_2)_{Adj}$	63	49.8 ± 1.6	49.3–50.4	44.7–52.0	50	48.5 ± 1.5	47.9–49.0	45.1–51.7
La/Yb	29	9.6 ± 3.8	7.6–11.6	3.4–20	16	12 ± 7	7–17	3–24
Ba/La	53	17 ± 8	14–20	7–50	40	16 ± 5	14–18	7–28
Ba/Zr	54	2.5 ± 2.3	1.7–3.4	1.1–15.9	41	3.0 ± 2.6	1.9–4.1	0.7–17.3
Ba/Nb	54	29 ± 19	22–36	10–131	41	26 ± 14	20–32	7–62
$LILE_E/LREE_E$	28	1.5 ± 0.5	1.3–1.7	1.1–3.3	11	1.34 ± 0.29	1.06–1.61	0.95–1.89
$LILE_E/HFSE_E$	54	2.6 ± 1.0	2.2–2.9	1.5–6.3	39	2.5 ± 1.0	2.1–2.9	1.1–5.2
				East-central segment				
$(SiO_2)_{Adj}$	27	51.0 ± 0.6	50.6–51.3	50.1–52.0	17	50.9 ± 0.8	50.3–51.5	49.1–52.0
La/Yb	12	7.9 ± 1.0	7.0–8.8	6.6–10.1	14	6.9 ± 1.2	5.9–7.9	5.2–9.3
Ba/La	22	16 ± 5	13–19	11–31	17	24 ± 10	17–31	11–49
Ba/Zr	23	2.0 ± 1.5	1.1–2.9	1.1–7.0	17	2.1 ± 1.0	1.4–2.7	0.9–4.0
Ba/Nb	14	80 ± 150	– 44–197	12–540	15	39 ± 21	22–55	17–88
$LILE_E/LREE_E$	10	1.41 ± 0.41	0.99–1.85	1.08–2.55	16	1.53 ± 0.34	1.28–1.78	0.82–2.13
$LILE_E/HFSE_E$	13	2.6 ± 1.6	1.2–4.0	1.6–6.6	15	2.2 ± 0.5	1.8–2.6	1.2–3.1
				West-central segment				
$(SiO_2)_{Adj}$	22	51.2 ± 0.6	50.8–51.6	49.2–51.9	17	50.2 ± 1.1	49.4–51.0	47.8–51.8
La/Yb	3	11 ± 9	– 40–63	4–21	3	11.9 ± 3.9	– 10.4–34.2	7.6–15.1
Ba/La	19	20 ± 8	15–25	12–39	13	15.4 ± 2.4	13.4–17.4	13–21
Ba/Zr	19	3.4 ± 1.6	2.4–4.4	1.7–6.3	13	2.15 ± 0.22	1.96–2.34	1.84–2.50
Ba/Nb	16	46 ± 21	31–62	18–82	13	18 ± 11	9–27	11–53
$LILE_E/LREE_E$	16	1.57 ± 0.34	1.31–1.82	1.12–2.30	13	1.30 ± 0.13	1.16–1.39	1.07–1.61
$LILE_E/HFSE_E$	16	3.4 ± 0.8	2.9–4.0	2.2–5.2	13	1.78 ± 0.41	1.42–2.12	1.43–3.02
				All segments				
$(SiO_2)_{Adj}$	112	50.4 ± 1.4	50.0–50.7	44.7–52.0	84	49.3 ± 1.7	48.8–49.8	45.1–52.0
La/Yb	44	9.3 ± 3.8	7.7–10.8	3.4–21.3	33	10 ± 5	7–12	3.4–23.6
Ba/La	94	17 ± 7	15–19	7–50	70	18 ± 7	15–20	7–49
Ba/Zr	96	2.6 ± 2.0	2.0–3.1	1.1–15.9	71	2.6 ± 2.1	2.0–3.3	0.7–17.3
Ba/Nb	84	40 ± 64	22–59	10–540	69	27 ± 17	22–32	7–88
$LILE_E/LREE_E$	54	1.50 ± 0.42	1.35–1.65	1.08–3.32	40	1.39 ± 0.29	1.27–1.52	0.82–2.13
$LILE_E/HFSE_E$	83	2.7 ± 1.1	2.4–3.1	1.5–6.6	67	2.3 ± 0.8	2.0–2.6	1.1–5.2
				Central American Volcanic Arc				
$(SiO_2)_{Adj}$	209	50.4 ± 1.1	50.2–50.6	46.4–52.0	20	50.2 ± 1.3	49.4–51.0	48.7–52.0
La/Yb	58	3.4 ± 1.0	3.1–3.8	1.9–6.3	20	7.2 ± 2.0	5.9–8.4	3.2–11.6
Ba/La	90	62 ± 28	54–70	20–130	20	26 ± 20	13–39	9–75
Ba/Zr	131	6.0 ± 2.9	5.4–6.7	1.0–14.5	19	3.6 ± 3.1	1.5–5.6	0.9–10.6
Ba/Nb	55	150 ± 140	102–203	11–620	16	45 ± 60	3–88	5–150
$LILE_E/LREE_E$	57	3.7 ± 1.2	3.3–4.1	1.5–6.0	20	1.9 ± 0.8	1.4–2.5	1.2–3.9
$LILE_E/HFSE_E$	54	5.2 ± 2.1	4.5–6.0	1.3–9.1	16	2.7 ± 2.0	1.2–4.2	1.1–6.0

n, Number of datapairs considered in the statistical calculations; *x*, Arithmetic mean value; *s*, Sample standard deviation value; 99% CL, Confidence limits of the mean value for the 99% confidence level; Range, Total range of values observed in a given segment or region. For the definition of segments, see Figure 2. CAVA data were compiled from the M. J. Carr's website (http://www-rci.rutgers.edu/~carr).

$LILE_E = (K_E + Rb_E + Ba_E + Sr_E)/4$ refers to the silicate earth-normalized value for selected alkali (K and Rb) and alkaline earth (Ba and Sr) elements.

$LREE_E = (La_E + Ce_E + Nd_E)/3$ refers to the silicate earth-normalized value for three light rare-earth elements (La, Ce and Nd).

$HFSE_E = (Nb_E + Zr_E + Ti_E + P_E)/4$ refers to the silicate earth-normalized value for selected high field strength elements (Nb, Zr, Ti and P).

The subscript *E* refers to normalization with respect to silicate earth values, for which all concentration data are normalized against silicate earth values given by McDonough and Sun[47]: K = 240; Rb = 0.600; Ba = 6.600; Sr = 19.9; La = 0.648; Ce = 1.675; Nd = 1.250; Nb = 0.658; Zr = 10.5; Ti = 1205; P = 90.

ing LILE enrichment with respect to HFSE) proposed in this work, because similar and overlapping 99%CL ranges (confidence limits at the 99% confidence level) are observed for 'front-arc' and 'back-arc' rocks (Table 2). If there were a significant contribution from the subduction process (Cocos plate), the 'front-arc' MVB magmas should show significantly lower values of La/Yb and higher values of all other key parameters than the 'back-arc' magmas, which is clearly not observed for this volcanic province (Table 2).

Further evidence against the subduction scenario comes from: (a) the significant differences between the MVB magmas (irrespective of whether from the 'front-arc' or 'back-arc') and the 'front-arc' CAVA magmas (Table 2) – all MVB magmas are, in fact, generally similar to the 'back-arc' CAVA magmas, which could be taken as an evidence for the MVB being situated in a 'back-arc' tectonic setting. However, such an affirmation would be meaningless because the nomenclature 'back-arc' necessarily requires an 'arc', which is shown to be absent in southern Mexico, i.e. there are no Miocene to Recent volcanoes between the MVB and the trench (Figure 1) that could be called an arc; (b) the similarities of the MVB magmas to those from several well-known modern rifts (for a synthesis of geochemical key parameters for rifts, see Verma[1]) – many of these compiled rifts, particularly the African rifts, have not been influenced by the subduction process throughout their geological history.

I, therefore, conclude that the origin of magmas in the MVB is related to ongoing extensional or rifting processes throughout the belt. Such a tectonic setting is possible because the MVB is sited along an ancient suture[48,49] and, according to Sheth *et al.*[9], mantle metasomatism was probably triggered passively by the formation of the lesion in the overlying plate and the development of a shallow, metasomatized, enriched mantle (inferred from the present inversion study) below the MVB, due to volatiles in a large region being drained through this narrow crack in the plate. This study further supports the conclusion by Verma[1] that there is no arc in southern Mexico related to the subduction of the Cocos plate.

Inverse modelling of geochemistry of basic rocks is a useful exercise to infer average source characteristics for magmas from the eastern to west-central MVB. An extensional or rift-related origin is confirmed by this methodology, rendering arc-related claims for the origin of the MVB magmas totally unsupported by results presented in this work.

1. Verma, S. P., Absence of Cocos plate subduction-related basic volcanism in southern Mexico: A unique case on earth? *Geology*, 2002, **30**, 1095–1098.
2. Carr, M. J., Feigenson, M. D. and Bennett, E. A., Incompatible element and isotopic evidence for tectonic control of source mixing and melt extraction along the Central American arc. *Contrib. Mineral. Petrol.*, 1990, **105**, 369–380.
3. Leeman, W. P., Carr, M. J. and Morris, J. D., Boron geochemistry of the Central American volcanic arc: Constraints on the genesis of subduction-related magmas. *Geochim. Cosmochim. Acta*, 1994, **58**, 149–168.
4. Verma, S. P. and Aguilar-Y-Vargas, V. H., Bulk chemical composition of magmas in the Mexican Volcanic Belt (Mexico) and inapplicability of generalized arc-models. *Chem. Erde*, 1988, **48**, 203–221.
5. Singh, S. K. and Pardo, M., Geometry of the Benioff zone and state of stress in the overriding plate in central Mexico. *Geophys. Res. Lett.*, 1993, **20**, 1483–1486.
6. Luhr, J. F., Extensional tectonics and the diverse primitive volcanic rocks in the western Mexican Volcanic Belt. *Can. Mineral.*, 1997, **35**, 473–500.
7. Márquez, A., Oyarzun, R., Doblas, M. and Verma, S. P., Alkalic (ocean-island basalt type) and calc-alkalic volcanism in the Mexican Volcanic Belt: A case for plume-related magmatism and propagating rifting at an active margin? *Geology*, 1999, **27**, 51–54.
8. Campos-Enríquez, J. O. and Sánchez-Zamora, O., Crustal structure across southern Mexico inferred from gravity data. *J. South Am. Earth Sci.*, 2000, **13**, 479–489.
9. Sheth, H. C., Torres-Alvarado, I. S. and Verma, S. P., Beyond subduction and plumes: a unified tectonic–petrogenetic model for the Mexican Volcanic Belt. *Int. Geol. Rev.*, 2000, **42**, 1116–1132.
10. Verma, S. P., Geochemistry of evolved magmas and their relationship to subduction-unrelated mafic volcanism at the volcanic front of the central Mexican Volcanic Belt. *J. Volcanol. Geotherm. Res.*, 1999, **93**, 151–171.
11. Verma, S. P., Geochemistry of the subducting Cocos plate and the origin of subduction-unrelated mafic volcanism at the volcanic front of the central Mexican Volcanic Belt. In *Cenozoic Tectonics and Volcanism of Mexico*. Geol. Soc. Am. Spec. Paper (eds Delgado-Granados, H. *et al.*), Boulder, Colorado, 2000, vol. 334, pp. 195–222.
12. Verma, S. P., Geochemical evidence for a lithospheric source for magmas from Los Humeros caldera, Puebla, Mexico. *Chem. Geol.*, 2000, **164**, 35–60.
13. Suter, M., López Martínez, M., Quintero Legorreta, O. and Carrillo Martínez, M., Quaternary intra-arc extension in the central Trans-Mexican Volcanic Belt. *Geol. Soc. Am. Bull.*, 2001, **113**, 693–703.
14. Velasco-Tapia, F. and Verma, S. P., First partial melting inversion model for a rift-related origin of the Sierra de Chichinautzin volcanic field, central Mexican Volcanic Belt. *Int. Geol. Rev.*, 2001, **43**, 788–817.
15. von Huene, R., The Middle America convergent plate boundary, Guatemala. In *The Eastern Pacific Ocean and Hawaii. The Geology of North America* (eds Winterer, E. L. *et al.*), Boulder, Colorado, 1989, pp. 535–550.
16. Luhr, J. F., Nelson, S. A., Allan, J. F. and Carmichael, I. S. E., Active rifting in southwestern Mexico: Manifestations of an incipient eastward spreading-ridge jump. *Geology*, 1985, **13**, 54–57.
17. Allan, J. F., Nelson, S. A., Luhr, J. F., Carmichael, I. S. E., Wopat, M. and Wallace, P. J., Pliocene–Holocene rifting and associated volcanism in southwest Mexico: An exotic terrane in the making. In *The Gulf and Peninsular Province of the Californias* (eds Dauphin, J. P. and Simoneit, B. R. T.), Am. Assoc. Petrol. Geol., 1991, pp. 425–445.
18. Otsuki, K., Kurokawa, K. and Hasenaka, T., Some characteristics of spatial distribution of volcanoes in the Michoacan–Guanajuato volcanic field, central Mexico. In Subduction volcanism and tectonics of western Mexican Volcanic Belt. International Scientific Research Program (No. 03041014) Japan–Mexico Co-operative Research. Faculty of Science (ed. Aoki, K.), Tohoku University, 1992, pp. 104–114.
19. Johnson, C. A. and Harrison, C. G. A., Neotectonics in central Mexico. *Phys. Earth Planet. Inter.*, 1990, **64**, 187–210.
20. Mooser, F., Montiel, A. and Zúñiga, A., Nuevo mapa geológico de las cuencas de México, Toluca y Puebla. Estratigrafía, tectónica

regional y aspectos geotérmicos. Comisión Federal de Electricidad, Mexico City, 1996, p. 25 + geologic maps.
21. Márquez, A., Oyarzun, R., de Ignacio, C. and Doblas, M., Southward migration of volcanic activity in the central Mexican Volcanic Belt: Asymmetric extension within a two-layer crustal stretching model. *J. Volcanol. Geotherm. Res.*, 2001, **112**, 175–187.
22. Luhr, J. F., Allan, J. F., Carmichael, I. S. E., Nelson, S. A. and Hasenaka, T., Primitive calc-alkaline and alkaline rock types from the western Mexican Volcanic Belt. *J. Geophys. Res.*, 1989, **94**, 4515–4530.
23. Verma, S. P. and Nelson, S. A., Isotopic and trace element constraints on the origin and evolution of alkaline and calc-alkaline magmas in the northwestern Mexican Volcanic Belt. *J. Geophys. Res.*, 1989, **94**, 4531–4544.
24. Molnar, P. and Sykes, L. R., Tectonics of the Caribbean and Middle America regions from focal mechanisms and seismicity. *Geol. Soc. Am. Bull.*, 1969, **80**, 1639–1684.
25. Negendank, J. F. W., Emmermann, R., Krawczyk, R., Mooser, F., Tobschall, H. and Werle, D., Geological and geochemical investigations on the eastern Trans Mexican Volcanic Belt. In Mexican Volcanic Belt – Part 2. *Geofís. Int.* (ed. Verma, S. P.), 1985, **24**, 477–575.
26. Suárez, G. and Singh, S. K., Tectonic interpretation of the Trans-Mexican Volcanic Belt – discussion. *Tectonophysics*, 1986, **127**, 155–160.
27. Hochstaedter, A. G., Ryan, J. G., Luhr, J. F. and Hasenaka, T., On B/Be ratios in the Mexican Volcanic Belt. *Geochim. Cosmochim. Acta*, 1996, **60**, 613–628.
28. Chesley, J., Ruiz, J., Righter, K., Ferrari, L. and Gomez-Tuena, A., Source contamination versus assimilation: An example from the Trans-Mexican Volcanic Arc. *Earth Planet. Sci. Lett.*, 2002, **195**, 211–221.
29. Wallace, P. J. and Carmichael, I. S. E., Quaternary volcanism near the Valley of Mexico: implications for subduction zone magmatism and the effects of crustal thickness variations on primitive magma compositions. *Contrib. Mineral. Petrol.*, 1999, **135**, 291–314.
30. Torres-Alvarado, I. S. and Verma, S. P., Comment to 'Neogene volcanism at the front of the central Mexican Volcanic Belt: basaltic andesites to dacites, with contemporaneous shoshonites and high-TiO_2 lava' by Blatter, D. L., Carmichael, I. S. E., Deino, A. L. and Renne, P. R., *Geol. Soc. Am. Bull.*, 2003, **115**, 1020–1021.
31. Siebert, L. and Carrasco-Núñez, G., Late-Pleistocene to precolumbian behind-the-arc mafic volcanism in the eastern Mexican Volcanic Belt; implications for future hazards. *J. Volcanol. Geotherm. Res.*, 2002, **115**, 179–205.
32. Gómez-Tuena, A., LaGatta, A. B., Langmuir, C. H., Goldstein, S. L., Ortega-Gutiérrez, F. and Carrasco-Núñez, G., Temporal control of subduction magmatism in the eastern Trans-Mexican Volcanic Belt: mantle sources, slab contributions, and crustal contamination. *Geochem. Geophys. Geosys.*, 2003, **4**, 10.1029/2003GC000524.
33. Verma, S. P., Geochemical and Sr-Nd-Pb isotopic evidence for a combined assimilation and fractional crystallisation process for volcanic rocks from the Huichapan caldera, Hidalgo, Mexico. *Lithos*, 2001, **56**, 141–164.
34. Verma, S. P., Geochemical evidence for a lithospheric source for magmas from Acoculco caldera, Eastern Mexican Volcanic Belt. *Int. Geol. Rev.*, 2001, **43**, 31–51.
35. Verma, S. P., Geochemical evidence for a rift-related origin of bimodal volcanism at Meseta Río San Juan, North-Central Mexican Volcanic Belt. *Int. Geol. Rev.*, 2001, **43**, 475–493.
36. Ferriz, H. and Mahood, G. A., Strong compositional zonation in a silicic magmatic system: Los Humeros, Mexican Neovolcanic Belt. *J. Petrol.*, 1987, **28**, 171–209.
37. Hasenaka, T., Chemical compositions of selected samples. In ref. 18, pp. 238–247.
38. Besch, T., Verma, S. P., Kramm, U., Negendank, J. F. W., Tobschall, H. J. and Emmermann, R., Assimilation of sialic crustal material by volcanics of the easternmost extension of the Trans-Mexican Volcanic Belt: Evidence from Sr and Nd isotopes. *Geofís. Int.*, 1995, **34**, 263–282.
39. Verma, S. P., Magma genesis and chamber processes at Los Humeros caldera, Mexico – Nd and Sr isotope data. *Nature*, 1983, **301**, 52–55.
40. Blatter, D. L., Carmichael, I. S. E., Deino, A. L. and Renne, P. R., Neogene volcanism at the front of the central Mexican volcanic belt: basaltic andesites to dacites, with contemporaneous shoshonites and high-TiO_2 lava. *Geol. Soc. Am. Bull.*, 2001, **113**, 1324–1342.
41. Verma, S. P. and Hasenaka, T., Sr, Nd, and Pb isotopic and trace element geochemical constraints for a veined-mantle source of magmas in the Michoacán–Guanajuato volcanic field, west-central Mexican Volcanic Belt. *Geochem. J.*, 2004, **38**, 43–65.
42. Hofmann, A. W. and Feigenson, M. D., Case studies on the origin of basalt. I. Theory and reassessment of Grenada basalts. *Contrib. Mineral. Petrol.*, 1983, **84**, 382–389.
43. Ormerod, D. S., Rogers, N. W. and Hawkesworth, C. J., Melting in the lithospheric mantle: Inverse modelling of alkali–olivine basalts from the Big Pine volcanic field, California. *Contrib. Mineral. Petrol.*, 1991, **108,** 305–317.
44. Feigenson, M. D. and Carr, M. J., The source of Central American lavas: Inferences from geochemical inverse modeling. *Contrib. Mineral. Petrol.*, 1993, **113**, 226–235.
45. Cebría, J. M. and López-Ruiz, J., A refined method for trace element modelling of nonmodal batch partial melting processes: the Cenozoic continental volcanism of Calatrava, central Spain. *Geochim. Cosmochim. Acta*, 1996, **60**, 1355–1366.
46. Caroff, M., Maury, R. C., Guille, G. and Cotten, J., Partial melting below Tubuai (Austral Islands, French Polynesia). *Contrib. Mineral. Petrol.*, 1997, **127**, 369–382.
47. McDonough, W. F. and Sun, S. -S., The composition of the earth. *Chem. Geol.*, 1995, **120**, 223–253.
48. De Cserna, Z., Orogenesis in time and space in Mexico. *Geol. Rundsch.*, 1960, **50**, 595–605.
49. Cebull, S. E. and Shurbet, D. H., Mexican Volcanic Belt: an intraplate transform? *Geofís. Int.*, 1987, **26**, 1–13.

Received 16 July 2003; revised accepted 13 November 2003

Additional information on palynological dating of Chhongtash Formation in eastern Karakoram and its palaeogeographical significance

Anshu K. Sinha, Neerja Jha* and Rajeev Upadhyay
Birbal Sahni Institute of Palaeobotany, 53 University Road, Lucknow 226 007, India

Palynological studies were carried out on additional samples of marine sedimentary succession of Chhongtash Formation, in eastern Karakoram, India. The present study revealed the presence of Lower Gondwana (Early Permian Asselian–Sakmarian) palynomorphs.

*For correspondence. (e-mail: neerjajha@yahoo.co.uk)